
Article:
Sims, Mark Timothy orcid.org/0000-0001-9438-5527, Abbott, Laurence Colin, Cowling, Stephen James orcid.org/0000-0002-4771-9886 et al. (2 more authors) (2016) Molecular Design Parameters of Anthraquinone Dyes for Guest-Host Liquid-Crystal Applications:Experimental and Computational Studies of Spectroscopy, Structure and Stability. Journal of Physical Chemistry C. 11151–11162. ISSN 1932-7455

https://doi.org/10.1021/acs.jpcc.6b03607

Molecular Design Parameters of Anthraquinone Dyes for Guest-Host Liquid-Crystal Applications: Experimental and Computational Studies of Spectroscopy, Structure and Stability

Mark T. Sims, Laurence C. Abbott, Stephen J. Cowling, John W. Goodby and

John N. Moore*

Department of Chemistry, The University of York, Heslington, York YO10 5DD, UK

Email address: john.moore@york.ac.uk

ABSTRACT:

A set of five anthraquinone dyes with bis-(4-propylphenyl) substituent groups, connected via sulfide or amine linkages at the 1,5-positions or directly at the 2,6-positions, have been studied in solution by UV-visible spectroscopy and electrochemistry, allied with density functional theory (DFT) calculations of structures, electronic transitions and redox potentials. The visible transitions and redox potentials are shown to vary with the HOMO and LUMO energies, with the variation in both colour and redox stability between the dyes being attributable principally to variations in the HOMOs located mainly on the substituents and outer anthraquinone rings. The calculated molecular structures and visible transition dipole moments are shown to vary subtly with substituent, giving variations in the molecular aspect ratios, minimum moment of inertia axes, and transition dipole moment vector orientations that can rationalise the alignment trends reported in the literature for such anthraquinone dyes in liquid crystal hosts, and showing why 1,5-disulfide and 2,6-diphenyl substituents give better designs than1,5-diamine substituents. The computational approaches reported here are shown to give good matches with experimental trends, indicating that they may be used more generally to aid the rational molecular design of dyes for applications as guests in liquid crystal hosts.

INTRODUCTION

The incorporation of a suitable dye into a liquid crystal host can result in the guest dye molecules aligning within the host.[1] Such guest-host systems have received significant attention because they offer the potential for many applications,[2-8] with the principal interest being in display devices in which the system can be switched between absorbing (coloured) and transmitting (clear) states by the application of an electric field that changes the molecular orientation of the material and hence the alignment of the dye molecules relative to the incident light.[9-11] In comparison with conventional liquid crystal colour displays that require the use of coloured filters, crossed polarisers and back-lighting, such guest-host devices offer the potential for significantly better energy efficiency and brightness, including the ability to operate without a polariser, and in a light-scattering mode in outdoor environments.[12-13]

Many different modes of operation for such guest-host devices have been successfully developed and tested since they were first demonstrated in the 1960s,[1, 10, 14] but their widespread practical use has been limited severely by the lack of suitable dyes that meet the stringent criteria required for such applications. These criteria include pure dyes with UV-visible absorption spectra that can be tuned by accessible synthetic routes, along with high visible oscillator strengths and high solubilities in liquid crystal hosts, which in combination can generate guest-host systems with a range of intense colours; alternatively, the judicious use of several dyes concurrently can generate intense black mixtures. The stability of guest dyes is also essential, particularly for applications in display devices that may be required to retain their optical properties over an operational lifetime of several years; and other criteria may arise from the introduction of a guest dye affecting host liquid crystal properties such as viscosity, switching time, alignment, and phase transition temperatures.

The degree of molecular alignment is critical to any liquid crystal device, and for guest-host applications the dye molecules must be highly aligned within the host, for example to achieve a high contrast ratio on switching between the absorbing and transmitting states of a device. The extent of molecular alignment in a liquid crystal is determined primarily by the molecular shapes and the nature of the intermolecular interactions;[15-16] the constituent molecules must be anisotropic, and a guest must also exhibit a significant degree of molecular anisotropy for alignment to occur within the host. The structure of the chromophoric group within a dye molecule typically has a significant influence on its overall molecular shape, and the rod-like shape of azo dyes led to their initial consideration as suitable guests within nematic liquid crystal hosts, which generally have rod-like molecular constituents.[17] Subsequently, many other types of dyes have been studied for use in such systems including tetrazines,[18] naphthalenes,[19-21] perylenes,[22] acenequinones [23] and anthraquinones.[24-26]

In addition to molecular alignment within a liquid crystal host, a suitable dye must also have a visible-wavelength electronic transition dipole moment (TDM) that is highly aligned with the molecular axis along which the dye aligns within the host because it is the reorientation of this TDM vector that determines the contrast ratio on switching, rather than the reorientation of the molecular axis of the dye.[27] The alignment of dye molecule TDMs in a guest-host system is generally quantified by an experimental dichroic order parameter *S*, for which a value of 1 indicates that the TDMs are fully aligned and a sample in which the TDMs exhibit no alignment gives a value of 0. This order parameter is derived from a dichroic ratio, $D = A_{\parallel} / A_{\perp}$, which is obtained by measuring the UV-visible absorbances of an aligned guest-host sample oriented parallel ($A_{\parallel}$) and perpendicular ($A_{\perp}$) to linearly polarized incident light. In a nematic liquid crystal, the constituent molecules align in a preferred direction called the director, **n**, and the alignment of the TDM vector of a dye against this director is shown

schematically in Figure 1, which gives this angle as ϕ and illustrates the concept that it may be split into two contributions: the alignment of the long molecular axis of the dye within the host given by the angle θ, and the alignment of the TDM with the long molecular axis of the dye given by the angle β. The molecules are not static and, in general, a dye molecule explores a distribution of θ angles that determines the overall molecular alignment, and the TDM explores a cone around the molecular axis, against which the β angle is generally taken to be fixed. The experimental dichroic order parameter S equates to S_ϕ, which arises from a distribution of angles ϕ, and which can be expressed as the product of two individual order parameters, S_θ arising from a distribution of θ angles, and S_β arising from a fixed β angle,[27] as given for a uniaxial system by eq 1,

$$S_\phi = S_\theta S_\beta = \left\langle \frac{1}{2}\left(3\cos^2\theta - 1\right)\right\rangle \left(\frac{1}{2}\left(3\cos^2\beta - 1\right)\right) \qquad (1)$$

where the angular brackets indicate an ensemble average. For some dyes, such as those with highly symmetric molecular structures, β may be approximately 0°, in which case the TDM alignment within the host is effectively defined only by the angles θ. However, for many dyes, and particularly for those with molecular structures of lower symmetry, β can be significant and may be the key factor in giving poor TDM alignment with the director and a low dichroic order parameter that renders a guest-host system unusable for practical devices.

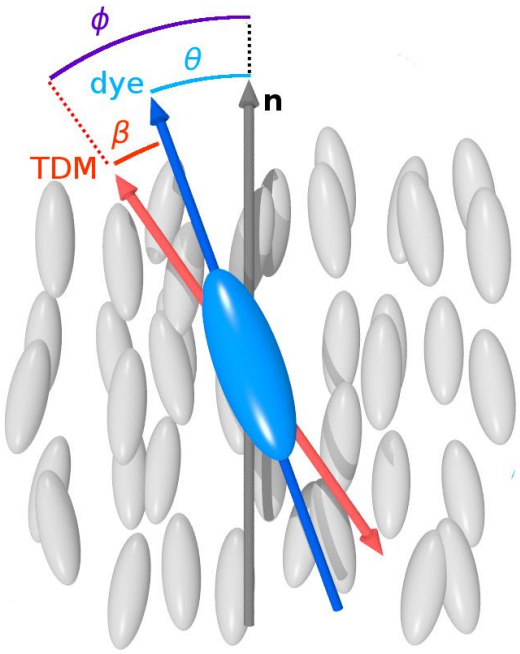

Figure 1. Schematic representation of a dye molecule (blue) within a nematic liquid crystal host (grey). The average orientation of the host molecules is given by the director, **n**, and the relative orientations of the long molecular axis of the dye (blue) and the TDM of the dye (red) are given with angles defined.

Since the guest-host effect was first demonstrated, many azo dyes have been studied in liquid crystal hosts, as reported in extensive patent as well as research literature, and significant effort has been invested in synthesising a wide variety of azo dyes to test for such applications. Many of these dyes have been designed with flexible hydrocarbon chains or other substituents, which can both enhance the rod-like nature of the molecular shape and improve compatibility with liquid crystals by mimicking the terminal groups (flexible chains) of the substituted biphenyl or similar molecular constituents of the host. Many of these azo dyes have been shown to align well within liquid crystal hosts,[17, 28] and they can provide a range of colours, but generally the potential of azo dyes for applications in practical guest-

host devices has been limited critically by their instability, and particularly by their poor photostability.[27, 29]

Similarly, the patent and research literature describes many 9,10-anthraquinone dyes that have been synthesised and studied for guest-host applications, often based on 1,5-disubstituted and 1,4,5,8-tetrasubstituted systems; a range of colours can be provided by varying the position and nature of the substituents[30] and, importantly, they have been shown generally to be much more stable than azo dyes.[27, 29] Many of these anthraquinone dyes have been shown to align well within liquid crystal hosts but the dichroic ratios have often been found to be lower than those of azo dyes,[26, 31] limiting their potential applications. In some cases, this effect has been suggested to arise from the choice and position of substituents resulting in poor alignment of the TDM with the long molecular axis of the anthraquinone dye giving a significant angle β.[27, 29] A recent report showed how a modest alteration in the structure of one substituent of a 1,5-disubstituted anthraquinone dye could give a significant improvement in its dichroic ratio in a liquid crystal host and in its contrast ratio on switching,[32] highlighting the importance of substituent design. Moreover, synthetic advances have recently enabled the synthesis of new 2,6-disubstituted anthraquinones that have more elongated and rod-like structures than 1,5-disubstituted systems,[33] and which may generally give higher alignments in liquid crystal hosts[34] due to substituent position being another important molecular design parameter.

It is evident that several design criteria relating to a number of interdependent properties must be met concurrently to produce a practical guest-host liquid crystal device. The starting point generally is to consider the design of liquid crystal hosts and dyes separately, and a primary limitation has been a lack of dyes that can meet the stringent criteria. Hence, it is desirable to develop a rational approach to dye design that is based on a

detailed knowledge and understanding of the interplay between the molecular structure and the properties that define the key parameters for such applications.

Of the two main classes of dyes that have been reported for guest-host applications, the azo class would generally seem to have better dichroic ratios but significant limitations arising from poor photostability, whereas the anthraquinone class would generally seem to have much better stability but lower dichroic ratios that the literature suggests might be improved by appropriate molecular design. Consequently, we have been studying the design of anthraquinone dyes for such applications. We recently reported the synthesis of five sets of very pure anthraquinone dyes with different colours, along with studies of their inherent liquid crystal phases and properties as pure dyes and as dye mixtures at elevated temperatures in the range 40-400 °C.[33] Subsequently, we have reported experimental and computational (density functional theory and molecular dynamics) studies of one of these dyes as a guest in a nematic liquid crystal host at room temperature.[34] Here, we report experimental and computational studies of the five dyes shown in Figure 2, which have terminal propyl substituents selected for consistency from the various terminal groups (propyl, hexyl, heptyl, etc.) that were synthesised within each set.[33] The three 1,5-disubstituted anthraquinones studied here (15SB3, 15NB3, 15NB3OH) are among a type that have been widely studied, including 15NB3 and close analogues of 15SB3 with slightly different terminal substituents,[24, 26, 31 35-38] and they are used here as exemplars of that type. The literature indicates that 1,5-dithiophenylanthraquinones, with the structure represented here by 15SB3, generally have higher order parameters ($S \approx 0.7$-0.8)[25-26, 31-32] in nematic liquid crystal hosts than 1,5-diaminophenylanthraquinones ($S \approx 0.6$-0.7),[24, 26, 31, 37] represented here by 15NB3. The two 2,6-disubstituted anthraquinones studied here (26B3, 26B3OH) have only recently been synthesised and have received limited studies to date,[33-34] and they are used here as

exemplars of this more rod-like type that might be expected generally to give high order parameters, as found in our recent study of 26SB3OH in the nematic host E7 (S = 0.74).[34]

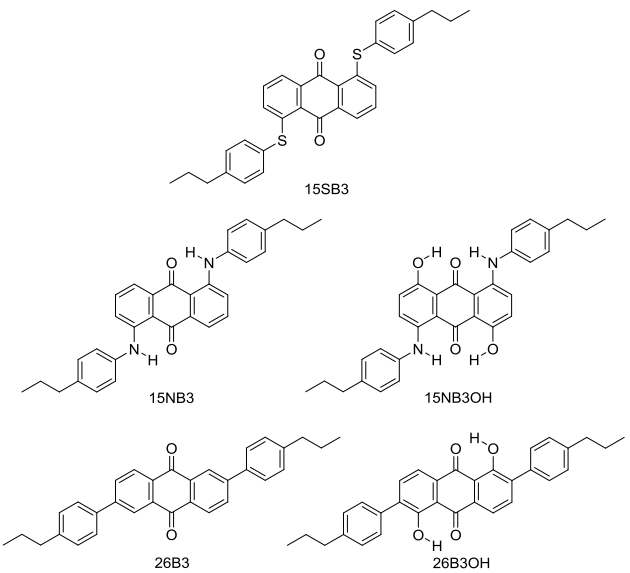

Figure 2. Structures of the dyes along with their abbreviations.

One aim of the study reported here was to develop an understanding of the interplay between the molecular structures and properties of these dyes in order to assess key design parameters that determine their potential suitability as guests in liquid crystal hosts. Another aim was to assess the ability of computational methods to provide an aid to the rational design of such dyes. In this article, we report on the influence of molecular design on the colours, spectra, molecular shapes, and stabilities of the five dyes by using a combination of experimental UV-visible spectroscopy and electrochemistry, allied with density functional theory (DFT) calculations including structures, spectra and redox potentials.

EXPERIMENTAL

The synthesis and purification of the dyes has been reported previously.[33] *p*-Xylene (>99%; Sigma-Aldrich), dichloromethane (>99.9%; Fisher), acetonitrile (anhydrous, 99.8%; Sigma-

Aldrich), tetrabutylammonium hexafluorophosphate (>99%; Sigma-Aldrich) and duroquinone (97%; Sigma-Aldrich) were used as received.

UV-visible absorption spectra of the dyes at ca. 2×10^{-4} mol dm^{-3} in *p*-xylene solution were recorded versus solvent, using matched quartz cuvettes (1 mm) and a Hitachi U-3010 spectrophotometer. The spectroelectrochemical studies used a custom cell consisting of a Pt gauze working electrode in a 1 mm pathlength quartz cell, a Pt wire counter electrode, and silver wire pseudo-reference electrode. A potentiostat (EG&G Princeton Applied Research 273) was used to control the potential, and the sample was left to equilibrate for 10 min after each change in potential, prior to recording a spectrum. The spectra were recorded from dyes at ca. 5×10^{-5} mol dm^{-3} in acetonitrile (or approaching saturation concentration where the solubility limit was lower) with tetrabutylammonium hexafluorophosphate at 0.1 mol dm^{-3} as the electrolyte, and they were baseline corrected; the solutions were purged initially for 15 min with nitrogen and remained under a flowing solvent-saturated nitrogen atmosphere for the duration of the experiments. All redox potentials are reported vs the ferrocene/ferricenium (Fc/Fc^+) redox couple,[39] which was recorded from a sample of ferrocene at 5×10^{-5} mol dm^{-3} in acetonitrile using the same spectroelectrochemical method; non-linear regression analyses of spectroelectrochemical data were performed using R.[40] All spectra were recorded at ca. 295 K.

DFT calculations were performed using the Gaussian 09 software package.[41] The structural optimisations were carried out using the B3LYP functional[42-43] with the 6-31G(d) basis set, and these optimised geometries were then used for the subsequent time-dependent DFT (TD-DFT) calculations that were carried out at the same level of theory. These calculations were performed on isolated molecules, and with the terminal propyl groups in all-*trans* configurations. Calculated UV-visible absorption spectra were produced by applying a Gaussian function (50 nm FWHM) to each calculated transition, scaled to the respective

calculated oscillator strength. The method for calculating the electrode potentials is described in the Results and Discussion section; in this case, the calculated standard Gibbs energies were obtained from structures that had been optimised in an acetonitrile solvent field using the SMD solvation model.[44]

The axis of minimum moment of inertia was defined as the eigenvector associated with the minimum eigenvalue of the inertia tensor for each optimised structure.[45] Aspect ratios were calculated from distances on the van der Waals surfaces of the optimised structures: the length was defined as the maximum distance between points on the van der Waals surface measured parallel with the axis of minimum moment of inertia, and the width was defined as twice the distance from the axis of minimum moment of inertia to the point on the van der Waals surface at the maximum distance perpendicular to that axis. These calculations were performed with in-house software.

RESULTS AND DISCUSSION

Colour and UV-visible spectroscopy. The five dyes exhibit a range of colours, as illustrated by the photograph in Figure 3 and as indicated by the UV-visible absorption spectra in Figure 4. In each case, the colour arises from a single strong visible absorption band with an absorption coefficient of $\varepsilon_{max} \geq 1 \times 10^4$ dm^3 mol^{-1} cm^{-1}, as listed in Table 1.

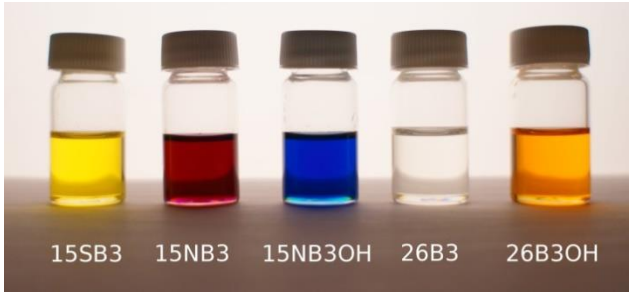

Figure 3. A photograph of solutions of the dyes at ca. 2 ×10^{-4} mol dm^{-3} in *p*-xylene.

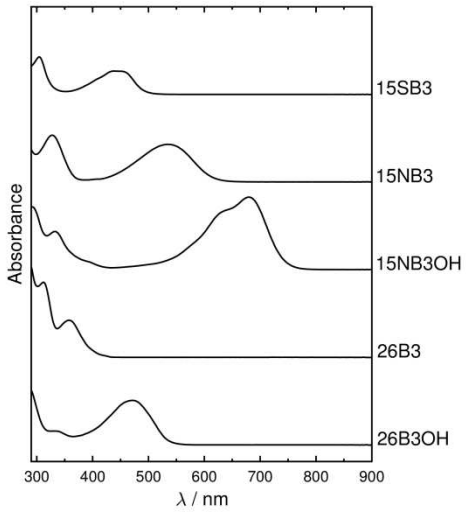

Figure 4. UV-visible absorption spectra of solutions of the dyes at ca. 2 × 10^{-4} mol dm^{-3} in *p*-xylene.

Table 1. Experimental visible absorption maxima (λ_{max}), energies (E_{max}), absorption coefficients (ε_{max}) and oscillator strengths (f) of the dyes in *p*-xylene alongside the calculated visible absorption transition wavelengths, energies and oscillator strengths for isolated molecules.

Dye	Experimental				Calculated		
	λ_{max} / nm	E_{max} / eV	ε_{max} / 10^4 dm^3 mol^{-1} cm^{-1}	f	λ / nm	E / eV	f
15SB3	439	2.82	1.05	0.14	453	2.74	0.28
15NB3	535	2.32	1.70	0.21	552	2.25	0.35
15NB3OH	680	1.82	3.51	0.32	634	1.96	0.55
26B3	358	3.46	1.71	0.18	390[a]	3.18	0.29[a]
26B3OH	471	2.63	2.04	0.28	492	2.52	0.57

[a]a weaker transition is also calculated for 26B3 at 385 nm (E = 3.22 eV; f = 0.07)

In the case of 26B3, 15SB3 and 15NB3, the colour variation may be rationalised qualitatively in terms of the electronic nature of the substituents, with a change from phenyl to sulfide to amine substituent corresponding to an increase in the electron-donating character giving a shift in the visible absorption maximum to longer wavelength.[46-47] In the case of the two hydroxyl-substituted dyes, 15NB3OH and 26B3OH, the addition of the hydroxyl groups in each case results in a >100 nm red-shift of the visible band compared with the dyes without the hydroxyl groups, which again is consistent with an increase in the electron-donating character of the substituents.

The DFT optimised structures of the dyes were used for TD-DFT calculations, which gave the calculated visible wavelength transitions listed in Table 1. The calculated absorption spectra derived from the TD-DFT calculations are shown in Figure 5, and exhibit a good overall match with the experimental band positions shown in Figure 4. Table 1 also includes the calculated oscillator strengths and the experimental oscillator strengths determined as $f = (k/n) \int \varepsilon(\tilde{\nu})\, d\tilde{\nu}$,[48] where the constant $k = 4.32 \times 10^{-9}$ cm mol dm^{-3} and the refractive index n = 1.5 for *p*-xylene. Although the calculated oscillator strengths are larger than those obtained

experimentally, the trend is replicated well between the experimental and calculated values, providing support for the optimised structures and illustrating the capability of TD-DFT calculations to predict trends for these systems.

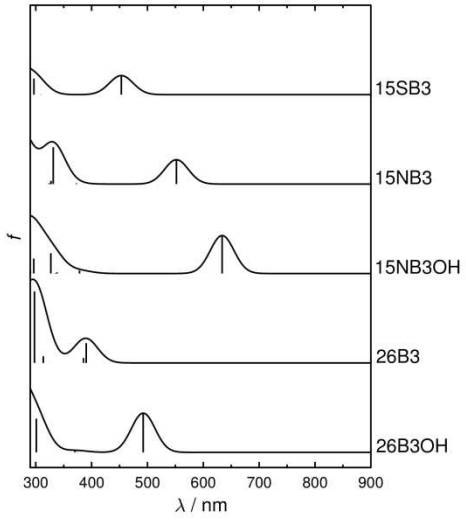

Figure 5. Calculated UV-visible absorption spectra and the underlying transitions indicated by vertical lines for each dye.

The TD-DFT calculations indicate that the visible bands of the dyes arise due to single HOMO → LUMO transitions, except for 26B3 where the strongest visible transition is due to a HOMO−1 → LUMO transition that is accompanied by a weaker transition of mixed orbital nature at slightly higher energy. These transitions are predominantly $\pi \rightarrow \pi^*$ intramolecular charge transfer in character for all of the dyes, as can be seen from the orbitals shown in Figure 6. In all cases, the orbitals from which the transitions originate are mainly located on the outer anthraquinone rings and their substituents, whereas the LUMOs are mainly located on the central anthraquinone rings and carbonyl groups; the transitions involve similar pairs of orbitals for all the dyes.

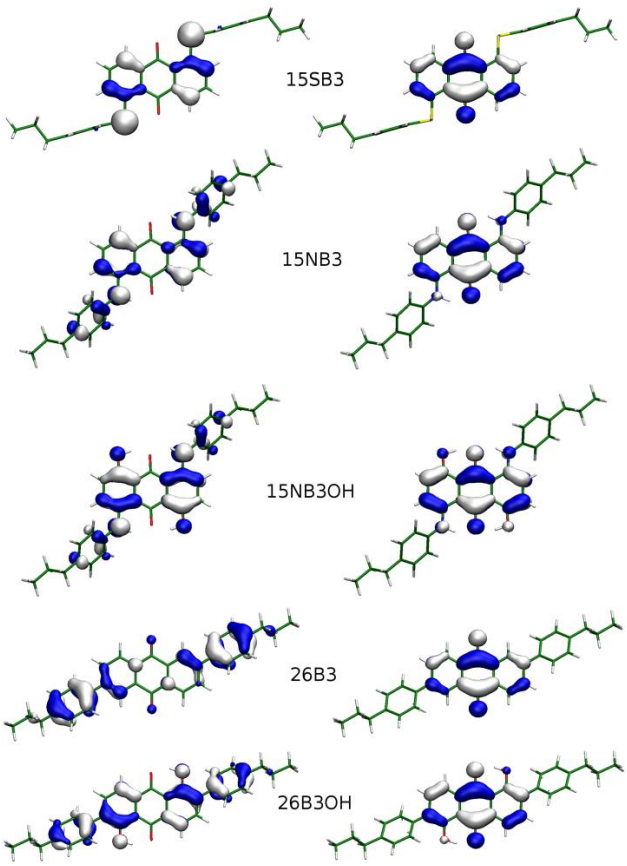

Figure 6. Optimised structures of the dyes and the orbitals involved in the visible transitions: HOMOs (left) and LUMOs (right) are shown except in the case of 26B3 for which the HOMO−1 and LUMO are shown.

The changes in electron density arising from these transitions were also calculated, as shown in Figure 7. These plots again show consistency between the dyes, and indicate that the visible transitions are due to shifts in electron density mainly from the substituents to the carbonyl groups.

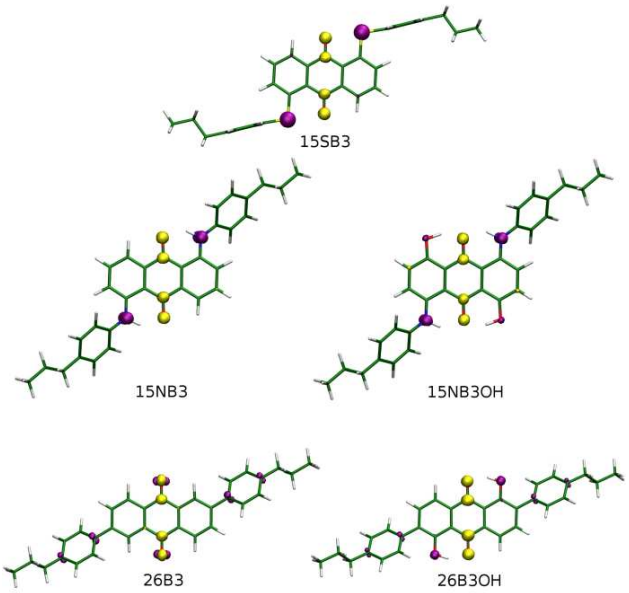

Figure 7. Optimised structure of the dyes and calculated changes in electron density on visible excitation: the shift occurs from the regions shown in purple to the regions shown in yellow; a cutoff threshold of ±0.007 *e* $Bohr^{-3}$ was used.

Molecular shape. The optimised structures of all five dyes have essentially planar anthraquinone cores but there are subtle variations in the calculated lowest energy conformations, as shown in Figure 6. The most noticeable variation is in the orientations of the phenyl substituents, which are shown more clearly in Figure 8; their planes lie at 90° to the plane of the anthraquinone core in the sulfide substituted dye, 15SB3, at 45° in both amine substituted dyes, 15NB3 and 15NB3OH, and at 35° and 41° in the direct phenyl substituted dyes, 26B3 and 26B3OH, respectively. These calculated angles are comparable with those of ca. 60° and 30° measured from crystal structures of 15NB3 and 26B3 analogues with hydrogens instead of terminal propyl groups,[49-51] and the differences may be attributable to comparing experimental geometries obtained from crystal structures with calculated gas-phase structures.

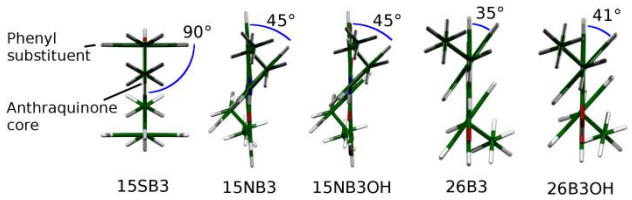

Figure 8. End-views of the optimised structures of the dyes showing the angle made between the plane of the anthraquinone core (drawn vertically in each case) and the plane of the phenyl substituents for each of the dyes.

The optimised structures of the dyes in Figure 6 show their rod-like structures, which can also be seen from the van der Waals surfaces in Figure 9 that were used to calculate the molecular dimensions. The minimum moment of inertia (MOI) axis, which is commonly used to define the axis of molecular alignment in liquid crystal studies,[16, 52] was used to define the axis along which the molecular length was measured (see Experimental section), as shown in Figure 9. The calculated molecular lengths and widths are listed in Table 2 along with the resultant aspect ratios, and the variation between the dyes is shown graphically in Figure 10. Equivalent calculations on dyes in which the terminal propyl groups were replaced with hydrogen atoms showed the same trend in aspect ratios (see Table S1 and Figure S1 in the Supporting Information), indicating that the variation in aspect ratio between the dyes is due to the differences in the nature of the anthraquinone substituents rather than the specific conformations or lengths of the terminal propyl chains on the phenyl substituent groups.

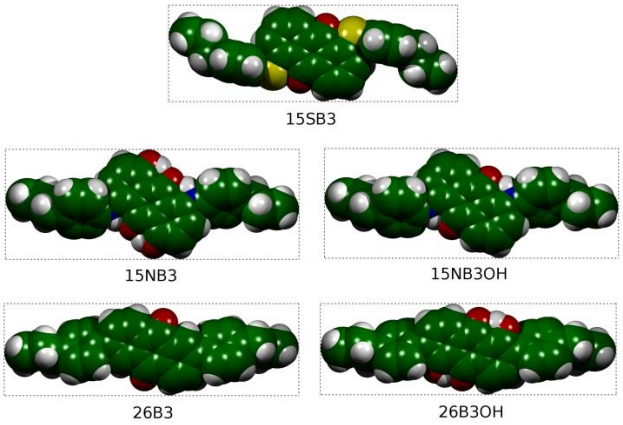

Figure 9. Optimised structures of the dyes showing the van der Waals radii of the atoms, with dashed boxes indicating the molecular lengths and widths defined by the van der Waals surfaces.

Table 2. Lengths and widths of the dyes determined from the van der Waals surfaces parallel and perpendicular to the minimum MOI axes, respectively, along with the resultant aspect ratios.

Dye	Length / Å	Width / Å	Aspect ratio
15SB3	26.44	8.84	2.99
15NB3	26.93	10.13	2.66
15NB3OH	26.92	10.62	2.53
26B3	26.99	8.48	3.18
26B3OH	27.10	8.37	3.24

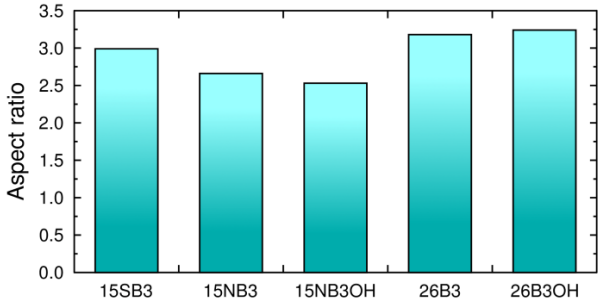

Figure 10. Aspect ratios of the dyes obtained from the van der Waals surfaces of the optimised structures.

Molecular aspect ratios have been used extensively to consider the degree of molecular alignment within liquid crystal systems, with higher ratios generally giving better alignment. For example, aspect ratios may be used to rationalise the subtle variation in order parameters of cyanobiphenyls with increasing alkyl chain length,[53] and they have been used widely as a variable in coarse-grain molecular dynamics simulations exploring the effects of overall molecular shape.[54-58] In the context of guest dye molecules in a liquid crystal host, the aspect ratio may therefore be considered to relate to the degree of alignment of the guest molecules within the host, as expressed by the S_θ order parameter within eq 1, which arises from the angles θ (Figure 1).

The 2,6-disubstituted dyes have higher aspect ratios than the 1,5-disubstituted dyes, which is attributable to the more elongated shapes determined by the positions of substitution. Among the 1,5-disubstituted dyes, the sulfide dye has a higher aspect ratio than the amine dyes, which can be rationalised by the C-S-C bond angle of 102° being smaller than the C-N-C bond angles of 129° giving phenyl rings that lie closer to the long axis of the anthraquinone core in 15SB3 than in 15NB3 and 15NB3OH. Additionally, the phenyl rings lie perpendicular to the anthraquinone core in 15SB3, which also contributes to a decrease in molecular width in comparison with 15NB3 and 15NB3OH.

The addition of hydroxyl substituents on going from 15NB3 to 15NB3OH causes a decrease in aspect ratio that is attributable to the larger groups in the 4,8-positions giving an increase in molecular width. Conversely, the addition of hydroxyl substituents on going from 26B3 to 26B3OH causes an increase in aspect ratio. In this case, the larger groups in the 1,5-positions do not change the molecular dimensions directly but the relatively high mass of the oxygen atoms causes a slight change in the minimum MOI axis that determines the axes used to measure the dimensions, resulting in 26B3OH having both a longer length and a narrower width than 26B3.

The trend in the aspect ratios calculated here is broadly consistent with reported experimental order parameters, suggesting that such calculations may potentially be used to predict the molecular alignment properties of such dyes. For example, the experimental order parameter of 26B3OH in a nematic host[34] is high in comparison with those of many 1,5-disubstituted anthraquinones, consistent with its high aspect ratio, and the relatively low experimental order parameters reported generally for diamino anthraquinones[24, 26, 31] are consistent with the relatively low aspect ratios of the diamino dyes studied here.

When combined with the UV-visible absorption spectra of the dyes, the analysis reveals a subtle interplay between molecular shape and colour that may not be intuitive from a simple inspection of the structures of the dyes, and which may lead to improved strategies for molecular design. Notably, the addition of hydroxyl groups to 15NB3 to obtain longer wavelength absorption from 15NB3OH results in a less rod-like structure and potentially worse alignment (lower S_θ value) within a liquid crystal host, whereas the addition of hydroxyl groups to 26B3 to obtain longer wavelength absorption from 26B3OH results in a more rod-like structure and potentially better alignment (higher S_θ value) within a liquid crystal host.

Transition dipole moment alignment. The orientations of the transition dipole moments of the visible transitions listed in Table 1 were obtained from the TD-DFT calculations and are shown as red arrows in Figure 11, overlaid on the optimised structures of the dyes, and with the minimum MOI axes shown as blue arrows. These two vectors together define the angle β shown in Figure 1, and the alignment of the TDM with the long molecular axis is quantified conventionally by the order parameter S_β, given within eq 1.[29] The calculated β angles are listed in Table 3 along with the S_β values, and the variation between the dyes is shown graphically in Figure 12.

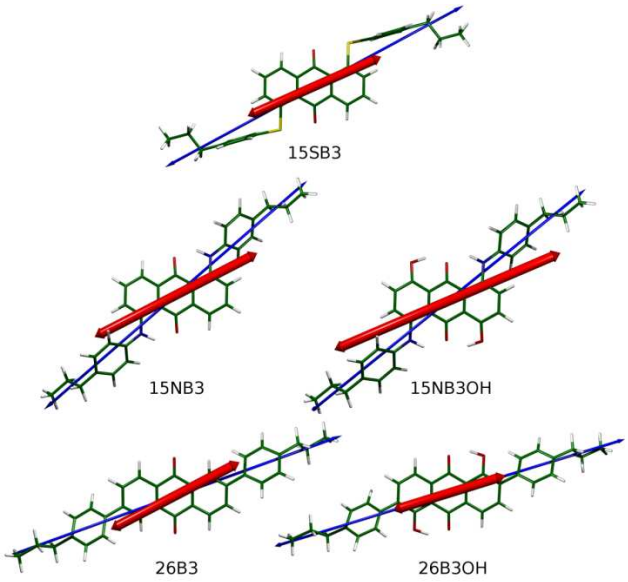

Figure 11. Optimised structures of the dyes with the orientations of the TDMs of the visible absorption transitions (red) and the minimum MOI axes (blue) overlaid.

Table 3. Calculated angles, β, between the visible TDMs and the minimum MOI axes of the dyes, and the respective order parameters, S_β.

Dye	β / °	S_β
15SB3	4.4	0.991
15NB3	13.8	0.914
15NB3OH	15.9	0.887
26B3[a]	8.4	0.968
26B3OH	1.7	0.999

[a]the weaker transition calculated at 385 nm gives $\beta = 8.8°$ and $S_\beta = 0.965$

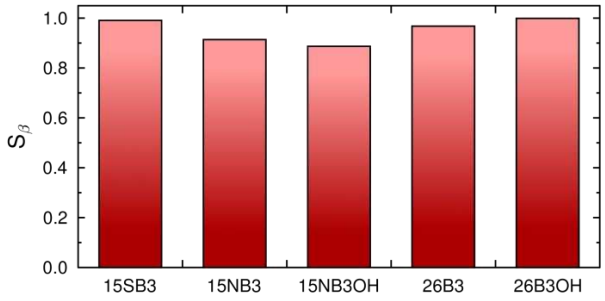

Figure 12. Order parameters, S_β, of the dyes calculated from the angles between the TDM orientations and the minimum MOI axes.

The TDMs of the two 2,6-diphenyl dyes and the 1,5-disulfide dye are well aligned with the respective minimum MOI axes, with both 26B3OH and 15SB3 giving very high order parameters of $S_\beta > 0.99$. By contrast, the two 1,5-amine dyes show poorer alignment.

The visible band is calculated to arise from a single transition for four of the dyes, giving only a single value of β to consider, whereas two transitions are calculated for 26B3. In the case of 26B3, the orientations of the two TDMs are very similar (Table 3) and the oscillator strength of the weaker transition is small (Table 1), such that the presence of a second transition is negligible, but this cannot be assumed in a general case and the presence of multiple transitions could have significant effects for other dyes.

The trend in the S_β values calculated here is broadly consistent with reported experimental order parameters that are generally higher for 2,6-disubstituted and 1,5-disubstituted sulfide anthraquinones than for 1,5-disubstituted amino anthraquinones.[24, 26, 31, 34] and hence, they are consistent with the TDM alignment within a host, defined by S_ϕ in eq 1, arising from S_β as well as S_θ. The calculated β and S_β values indicate that 2,6-disubstitution may provide an effective method of aligning the TDM with the long molecular axis (in addition to increasing the rod-like nature of the molecules, as discussed above), and they also provide an additional rationale for the higher experimental order parameters of sulfide versus amine 1,5-disubstituted anthraquinone dyes.

Redox stability. The redox stabilities of the dyes were studied in acetonitrile to provide a wide solvent window that enabled oxidation as well as reduction processes to be studied. UV-visible spectroelectrochemistry was used to monitor the processes because its high sensitivity and selectivity enabled the dyes to be studied at the low concentrations dictated by their limited solubility ($<10^{-4}$ mol dm^{-3}) in this solvent.

The UV-visible absorption spectra of the dyes in acetonitrile recorded at different applied potentials vs Fc/Fc^+ are shown in Figure 13; the changes arising from the applied

potentials can be seen by comparison with the spectra of the neutral dyes shown in Figure 4. Figure S2 in the Supporting Information shows the equivalent plots from ferrocene used for calibration. The spectral changes observed on the application of negative and positive potentials indicate that both reduction and oxidation processes are observed for each of the dyes. On reduction, each of the dyes exhibits an increase in absorbance at long wavelength, which is consistent with the behaviour of unsubstituted anthraquinone,[59] along with a decrease of the visible absorption band of the neutral dye. On oxidation, the visible absorption band of the dyes generally decreases, with no distinct visible absorption bands arising from the product(s) of oxidation. Insets to Figure 13 show plots of the absorbance against applied potential at selected wavelengths that showed significant changes and that were used for analysis; the reduction data were analysed at long wavelengths where new absorption bands arise, and the oxidation data were analysed at wavelengths corresponding to absorption bands of the neutral dyes.

The data were analysed according to the Nernst equation, $E = E^{o} - (RT/nF)\ln Q$, where E is the applied potential, E^{o} is the redox potential, R is the gas constant (8.314 J K^{-1} mol^{-1}), T is the temperature, F is the Faraday constant (9.649×10^{4} C mol^{-1}), n is the number of electrons transferred, and Q is the reaction quotient taken to be the concentration ratio of reduced and oxidised species, [Red]/[Ox]. As conventionally used in spectrochemical analysis,[60] the limiting absorbances are taken to arise from the oxidised and reduced species, A_{ox} and A_{red}, respectively, giving eq 2

$$A = \frac{A_{ox} + A_{red} e^{nF\left(E^{o} - E\right)/RT}}{1 + e^{nF\left(E^{o} - E\right)/RT}} \qquad (2)$$

which was used for the non-linear regression analyses shown in Figure 13. The redox potentials obtained from the fits are listed in Table 4. The fitted values of n were in the range

0.9 ± 0.6, and fits constrained to n = 1.0 gave similar fits and E^{o} values within 0.01 V of those listed in Table 4.

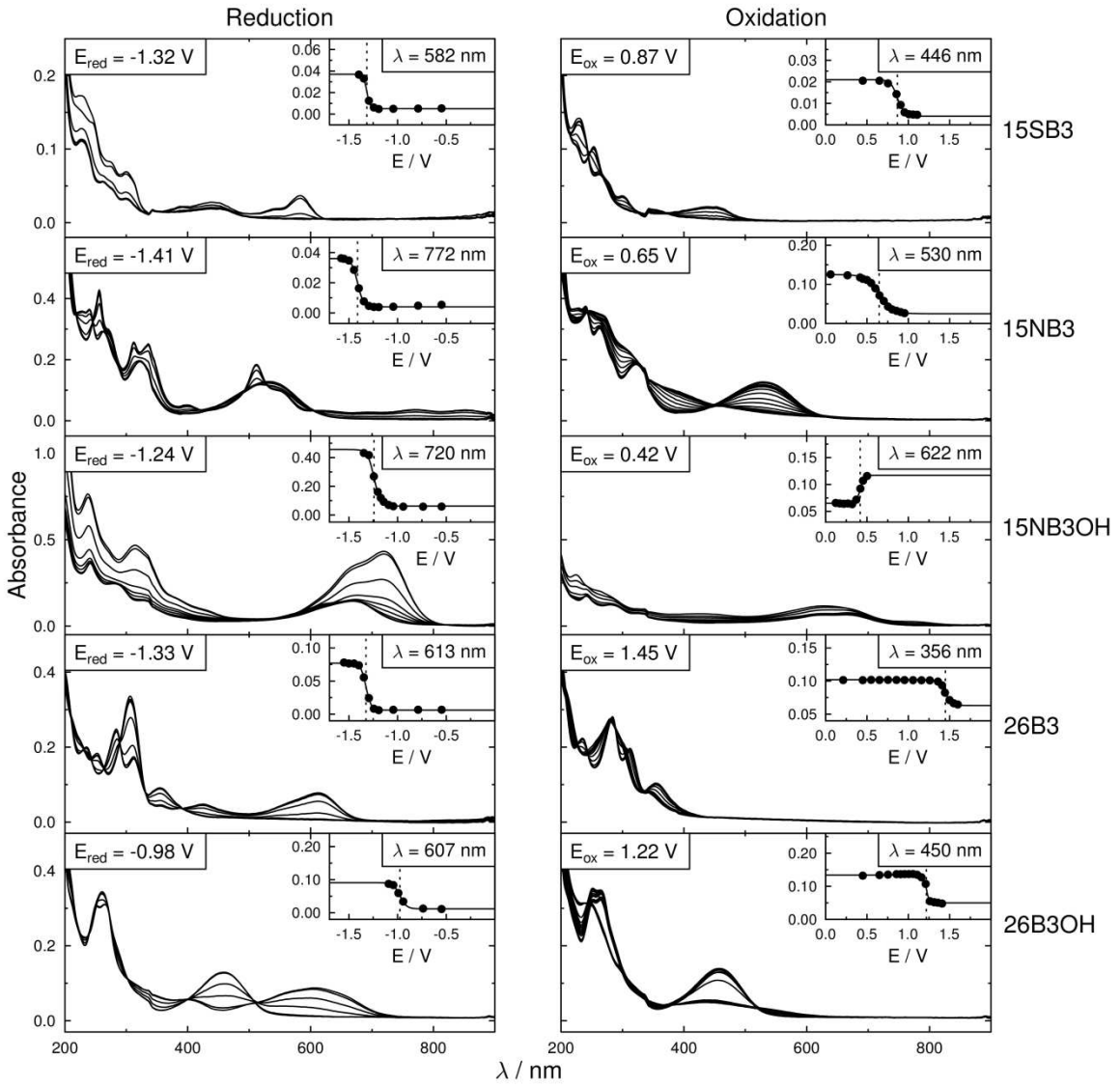

Figure 13. UV-visible absorption spectra of the dyes in acetonitrile on electrochemical reduction (left) and oxidation (right). The spectra were obtained at each of the applied potentials (•) indicated in the respective insets top right, which show plots of the absorbance at a selected single wavelength against applied potential and the fits to eq 2 (—) used to estimate the redox potentials vs Fc/Fc^{+}, with the dotted vertical lines indicating the potentials obtained from the fits, as given in the insets top left.

Table 4. Experimental redox potentials of the dyes in acetonitrile vs Fc/Fc^+ obtained from the spectroelectrochemical data, and their differences, ΔE, alongside calculated values vs Fc/Fc^+ obtained from DFT calculations on molecules in an acetonitrile solvent field and referenced against duroquinone.

Dye	$E_{(Dye, Dye^{\bullet -})}$ / V		$E_{(Dye^{\bullet +}, Dye)}$ / V		ΔE / V	
	exptl	calcd	exptl	calcd	exptl	calcd
15SB3	−1.32	−1.27	0.87	1.36	2.19	2.63
15NB3	−1.41	−1.29	0.65	0.78	2.06	2.07
15NB3OH	−1.24	−1.17	0.42	0.53	1.66	1.70
26B3	−1.33	−1.30	1.45	1.62	2.78	2.92
26B3OH	−0.98	−1.02	1.22	1.48	2.20	2.50

The redox stabilities of the dyes were also studied by cyclic voltammetry, using dichloromethane as the solvent to give the higher concentrations required due to the lower sensitivity, and these studies are reported in the Supporting Information. The cyclic voltammograms (Figure S3) gave E^o values in dichloromethane (Table S2) that showed essentially the same trends as observed for acetonitrile (Table 4), but the narrower solvent window precluded the observation of oxidation processes for most of the dyes.

A comparison of the redox potentials of the dyes shows that there is significantly more variation in the observed oxidation potentials than the reduction potentials, consistent with the natures of the HOMOs and LUMOs shown in Figure 6. The LUMOs to which an electron is added on reduction are located mainly on the central anthraquinone ring and carbonyl groups, and the comparable reduction potentials are attributable to the substituents having a relatively limited effect on these orbitals; the three dyes without hydroxyl groups show a small variation of ca. 0.09 V in the reduction potential, and the addition of the hydroxyl groups lowers the magnitude by ca. 0.2-0.3 V, consistent with intramolecular hydrogen bonding stabilising the anions.[61] By contrast, the HOMOs from which an electron is removed on oxidation are located mainly on the outer anthraquinone rings and their

substituents, and the greater variation of ca. 1.03 V in the oxidation potentials can be explained by a much stronger effect arising from the position and nature of these substituents. Considering the nature of the substituents, 26B3 has the least electron-donating phenyl groups, consistent with it exhibiting the highest oxidation potential, whereas 15NB3OH has the most electron-donating amino-phenyl and hydroxyl substituents and exhibits the lowest oxidation potential of these dyes. The trends in the redox potentials are discussed further below.

Redox potentials were calculated from the Gibbs energies of the cationic, neutral, and anionic forms of the dyes obtained from DFT optimised structures, in accordance with established methods.[61-63] The structures used to obtain the Gibbs energies were optimised in an acetonitrile solvent field, which is reported to be preferable to using structures optimised in the gas phase and subsequently calculating solvation energies;[64] and the potentials were calculated relative to those of a reference compound, rather than as absolute potentials, in order to remove the influence of systematic errors between the experimental conditions used here and those used to determine absolute potentials of reference compounds reported elsewhere.[65] Duroquinone (DQ), shown in Figure 14, was chosen as the reference compound because of its structural similarity to the dyes and its experimentally accessible oxidation and reduction potentials, which we measured to be +2.15 and −1.21 V vs Fc/Fc^+, respectively, using spectroelectrochemistry and the same conditions used for the dyes, as reported in the Supporting Information (Figure S4); these values are comparable to those reported for DQ under different experimental conditions.[66-67]

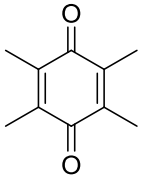

Figure 14. Structure of duroquinone (DQ).

Isodesmic reaction schemes for the reduction and oxidation of a dye with duroquinone as the reference compound are given as reactions 3 and 4 below, from which equations 5 and 6, respectively, are obtained using the relationship $\Delta G = -nFE$.

$$DQ\bullet^{-}_{(MeCN)} + Dye_{(MeCN)} \xrightarrow{\Delta G_{Red}} DQ_{(MeCN)} + Dye\bullet^{-}_{(MeCN)} \quad (3)$$

$$DQ\bullet^{+}_{(MeCN)} + Dye_{(MeCN)} \xrightarrow{\Delta G_{Ox}} DQ_{(MeCN)} + Dye\bullet^{+}_{(MeCN)} \quad (4)$$

$$\Delta G_{Red} = -nF\left(E_{(Dye,\ Dye^{\bullet -})} - E_{(DQ,\ DQ^{\bullet -})}\right) \quad (5)$$

$$\Delta G_{Ox} = -nF\left(E_{(DQ^{\bullet +},\ DQ)} - E_{(Dye^{\bullet +},Dye)}\right) \quad (6)$$

The DFT calculated Gibbs energies of the dye and duroquinone species (Table S3) were used in accordance with reactions 3 and 4 to obtain calculated ΔG values, which were then used in equations 5 and 6 along with our experimental values of $E_{(DQ,\ DQ^{\bullet -})}$ and $E_{(DQ^{\bullet +},\ DQ)}$ to obtain the calculated values of $E_{(Dye,\ Dye^{\bullet -})}$ and $E_{(Dye^{\bullet +},\ Dye)}$. These calculated redox potentials of the dyes are listed in Table 4 and are shown graphically in Figure 15 along with the experimental values.

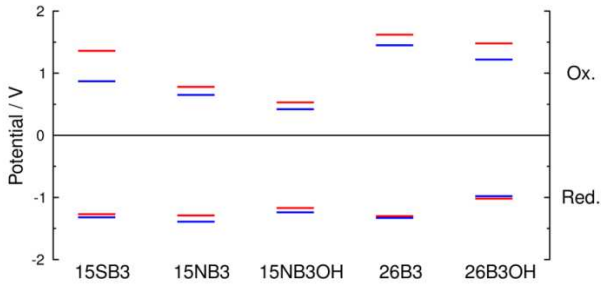

Figure 15. Experimental (blue) and calculated (red) oxidation and reduction potentials of the dyes in acetonitrile vs Fc/Fc^{+}.

A comparison shows that there is a good match between calculated and experimental redox potentials. The better match observed for the reduction than the oxidation potentials may be attributable to the use of duroquinone as the reference compound for the calculated values because it may be expected to give a better match for the LUMOs of the dyes, located on the central anthraquinone ring and carbonyl groups, than the HOMOs of the dyes, located on the outer anthraquinone rings and substituents. There is also a good match between the calculated and experimental differences between the oxidation and reduction potentials, ΔE, which are also listed in Table 4 and shown graphically in Figure 15, and which give the redox windows in which the dyes are electrochemically stable. The trend in the size of the redox windows matches the trend in the oxidation potentials of the dyes, which again is consistent with the change in the HOMOs being the primary cause of the variation in redox stability between the dyes.

Dye design. The experimental and computational results reported here demonstrate the interplay between molecular structures and key optical, redox and alignment properties that need to be tailored concurrently to design dyes that can be used in practical guest-host devices. This type of interplay may be expected to occur generally; here, it has been

demonstrated by studies of how the position and nature of substituents affects the properties of this set of anthraquinone dyes.

Both the redox stabilities and the observed colours of the dyes studied here are attributable to the HOMO and LUMO energies. Figure 16 shows the experimental HOMO and LUMO energies of the dyes estimated from the electrochemical data according to $E_{HOMO} = -(E_{ox} + 4.8)$ eV and $E_{LUMO} = -(E_{red} + 4.8)$ eV, respectively,[68-71] where −4.8 eV is the reported potential of Fc/Fc^+ vs the zero vacuum level. Figure 16 also shows the UV-visible absorption spectra of the dyes in *p*-xylene, plotted in eV relative to the HOMO energies, with arrows giving the transition energies to the experimental absorption peaks, along with schematic illustrations of the colours absorbed and the complementary colours observed from the dyes (as shown by the photograph in Figure 3). The inter-related nature of the redox and colour properties is illustrated schematically by Figure 16; for example, a large redox window correlates with a high-energy transition giving short-wavelength absorption in the violet and an observable yellow colour.

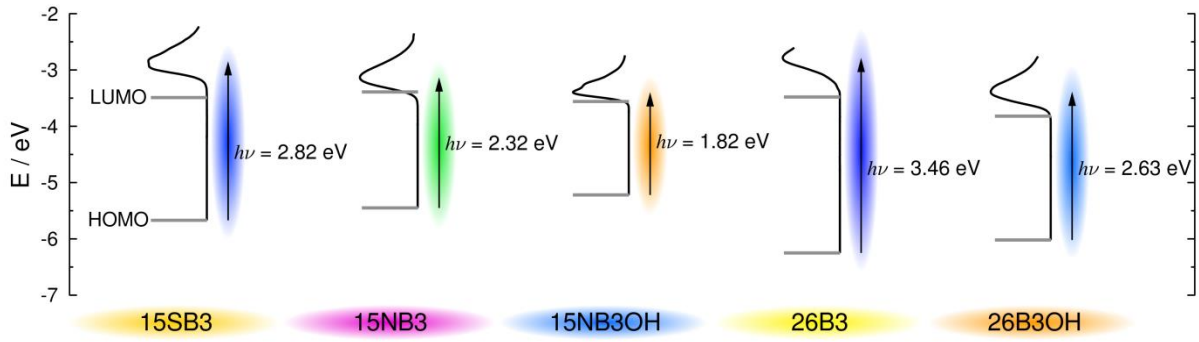

Figure 16. HOMO and LUMO energies estimated from experimental redox potentials with overlaid UV-vis absorption spectra in *p*-xylene plotted in eV relative to the respective HOMO energies of the dyes, to which the baselines are extended. The absorbed colours and the complementary colours observed from the dyes are illustrated schematically.

For the dyes studied here, it is evident that the substituents have only a small effect on the LUMO energies, and that a change in the substituents to give a longer wavelength visible transition arises from an increase in the HOMO energy that also narrows the redox window and lowers the stability towards oxidation. Consequently, to achieve long-wavelength absorption while maintaining relatively high stability to oxidation, it may be necessary to design an alternative chromophore in which the LUMO is of lower energy, or in which the energy of the LUMO may be tuned by substituents. The good match in experimental and computational trends reported here for both optical and electrochemical properties demonstrates the potential value of computational calculations to rationalise these trends and to provide an aid generally to molecular design for appropriate colour and redox stability.

As well as providing information on the stability of dyes towards oxidation and reduction in the ground state, redox potentials also provide a general starting point to consider photochemical redox stability because both oxidation and reduction reactions are more favourable in the excited state by approximately the electronic excitation energy. For anthraquinones, excited-state reduction reactions in particular are well-established to produced radical anions that participate in photochemical processes.[72]

Considering the alignment properties required for dyes to be used in guest-host systems, it is evident that even subtle changes in the molecular structure can cause significant changes in the molecular geometry, overall shape, and alignment of the TDM within the dye. The values calculated for the dyes studied here, illustrated in Figure 17, show that the 2,6-substituents give both high aspect ratios and small TDM angles that may be expected to give good contrast ratios in liquid crystal devices, whereas the 1,5-substituents give smaller aspect ratios and larger TDM angles for the amines that a change to sulfide substitution improves significantly. The contrasting effects of adding OH substituents to 15NB3 and 26B3 to give

worse and better designs, respectively, in terms of aspect ratio and TDM angle, highlight subtleties to be considered in substituent design. A comparison with reported experimental data suggests that the aspect ratios and β angles are both significant factors in the observed variation in order parameters for these types of dyes in liquid crystal hosts, and that such computational calculations may be a useful aid generally to this aspect of molecular design.

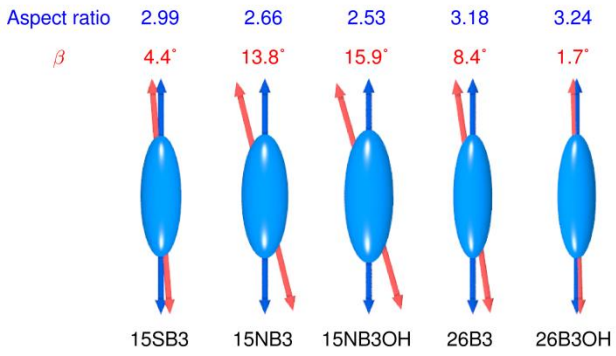

Figure 17. Calculated aspect ratios and angles β, between the TDM (red) and the minimum MOI axis (blue), with the dyes represented as ellipsoids (blue) at the respective aspect ratios.

CONCLUSIONS

Combined spectroscopic, electrochemical and computational studies of a set of five anthraquinone dyes have provided insights into the effects of molecular substituents on properties that are relevant for their applications as guests in liquid crystal hosts. The subtleties of structural variations have been highlighted, in particular the interdependent properties of colour, redox potentials, molecular shape, and TDM alignment, which can rationalise the variations in observed alignment reported in the literature for such dyes in liquid crystal hosts. The studies have demonstrated that straightforward substituent effects cannot be assumed due to the interdependence of the molecular properties and their sensitivity to the position and nature of the substituents on the anthraquinone core.

Specifically, the work reported here has shown that anthraquinones with 2,6-substituents give relatively high aspect ratios and TDM alignments that may be expected to offer a general route to improved molecular designs for liquid crystal applications, and has rationalised why 1,5-sulfide substituents can offer an alternative approach. In the present work, the dyes with these designs gave absorption bands in the UV-blue region that resulted in yellow-orange colours; the results suggest that new designs with different 2,6-substituents that generate longer wavelength absorption bands may offer a general route to blue and red dyes with better alignment properties than the class of 1,5-amino dyes studied here. Importantly, the computational approaches described here provide a valuable tool because they can be used not only to rationalise experimentally observed trends but also to assess key properties of hypothetical structures prior to synthesis being carried out, and they may be used generally as an aid to the rational molecular design of such dyes.

ACKNOWLEDGEMENT

This work was supported by an EPSRC DTA studentship (EP/J500598/1), EPSRC grant EP/M020584/1 for the development of dyes for liquid crystal applications, and EPSRC Platform Grant EP/D055261/1 and EPSRC grant EP/J007714/1 for the development of liquid crystals for displays. Additionally, we thank The Technology Partnership (UK) and Halation (China) for support on the development of the synthesis of dyes.

SUPPORTING INFORMATION

DFT calculated lengths, widths and apsect ratios of model dyes. Spectroelectrochemical data from ferrocene and duroquinone. Cyclic voltammetry data from the five dyes in dichloromethane. Calculated Gibbs energies.

REFERENCES

1. Heilmeier, G. H.; Zanoni, L. A., Guest-Host Interactions in Nematic Liquid Crystals . A New Electro-Optic Effect. *Appl. Phys. Lett.* **1968**, *13*, 91-92.

2. Peeters, E.; Lub, J.; Steenbakkers, J. A. M.; Broer, D. J., High-Contrast Thin-Film Polarizers by Photo-Crosslinking of Smectic Guest-Host Systems. *Adv. Mater.* **2006**, *18*, 2412-2417.

3. Lutfor, M. R.; Hegde, G.; Kumar, S.; Tschierske, C.; Chigrinov, V. G., Synthesis and Characterization of Bent-Shaped Azobenzene Monomers: Guest-Host Effects in Liquid Crystals with Azo Dyes for Optical Image Storage Devices. *Opt. Mater.* **2009**, *32*, 176-183.

4. Debije, M. G., Solar Energy Collectors with Tunable Transmission. *Adv. Funct. Mater.* **2010**, *20*, 1498-1502.

5. Liu, Q. K.; Beier, C.; Evans, J.; Lee, T.; He, S. L.; Smalyukh, I. I., Self-Alignment of Dye Molecules in Micelles and Lamellae for Three-Dimensional Imaging of Lyotropic Liquid Crystals. *Langmuir* **2011**, *27*, 7446-7452.

6. Saha, A.; Tanaka, Y.; Han, Y.; Bastiaansen, C. M. W.; Broer, D. J.; Sijbesma, R. P., Irreversible Visual Sensing of Humidity Using a Cholesteric Liquid Crystal. *Chem. Commun.* **2012**, *48*, 4579-4581.

7. Kendhale, A. M.; Schenning, A. P. H. J.; Debije, M. G., Superior Alignment of Multi-Chromophoric Perylenebisimides in Nematic Liquid Crystals and Their Application in Switchable Optical Waveguides. *J. Mater. Chem. A* **2013**, *1*, 229-232.

8. Contoret, A. E. A.; Farrar, S. R.; Jackson, P. O.; Khan, S. M.; May, L.; O'Neill, M.; Nicholls, J. E.; Kelly, S. M.; Richards, G. J., Polarized Electroluminescence from an Anisotropic Nematic Network on a Non-Contact Photoalignment Layer. *Adv. Mater.* **2000**, *12*, 971-974.

9. Heilmeier, G. H.; Zanoni, L. A.; Barton, L. A., Dynamic Scattering in Nematic Liquid Crystals. *Appl. Phys. Lett.* **1968**, *13*, 46-47.

10. White, D. L.; Taylor, G. N., New Absorptive Mode Reflective Liquid-Crystal Display Device. *J. Appl. Phys.* **1974**, *45*, 4718-4723.

11. Uchida, T.; Wada, M., Guest-Host Type Liquid-Crystal Displays. *Mol. Cryst. Liq. Cryst.* **1981**, *63*, 19-43.

12. Raj, D., Dichroic Display Technology Potentials and Limitations. *Mater. Chem. Phys.* **1996**, *43*, 204-211.

13. Gardiner, D. J.; Coles, H. J., Organosiloxane Liquid Crystals for Fast-Switching Bistable Scattering Devices. *J. Phys. D: Appl. Phys.* **2006**, *39*, 4948-4955.

14. Uchida, T.; Seki, H.; Shishido, C.; Wada, M., Bright Dichroic Guest-Host Lcds without a Polarizer. *Proc. SID* **1981**, *22*, 41-46.

15. Palsson, L. O., et al., Orientation and Solvatochromism of Dyes in Liquid Crystals. *Mol. Cryst. Liq. Cryst.* **2003**, *402*, 279-289.

16. Goodby, J. W., et al., Molecular Complexity and the Control of Self-Organising Processes. *Liq. Cryst.* **2009**, *36*, 567-605.

17. Seki, H.; Shishido, C.; Yasui, S.; Uchida, T., Dichroic Azo Dyes for Guest-Host Liquid-Crystal Cell. *Jpn. J. Appl. Phys., Part 1* **1982**, *21*, 191-192.

18. Pelzl, G.; Zaschke, H.; Demus, D., Liquid-Crystalline Tetrazine Compounds as Dyes for Guest-Host Displays with Positive Contrast. *Displays* **1985**, *6*, 141-147.

19. Wolarz, E.; Moryson, H.; Bauman, D., Dichroic Fluorescent Dyes for Guest-Host Liquid-Crystal Displays. *Displays* **1992**, *13*, 171-178.

20. Bauman, D.; Kuball, H. G., Uv-Visible Linear Dichroism of Naphthalene Bicarboxylic Acid-Derivatives Dissolved in Nematic Liquid-Crystal. *Chem. Phys.* **1993**, *176*, 221-231.

21. Martynski, T.; Mykowska, E.; Stolarski, R.; Bauman, D., Derivatives of 4-Amino-N-Ethylnaphthalimide for Use in Nematic Liquid-Crystals. *Dyes Pigm.* **1994**, *25*, 115-129.

22. Bauman, D.; Mykowska, E.; Wolarz, E., Molecular Orientation of Perylene-Like Dyes in Liquid Crystal 8OCB. *Mol. Cryst. Liq. Cryst. Sci. Technol., Sect. A* **1998**, *321*, 333-347.

23. Chen, Z. H.; Swager, T. M., Synthesis and Characterization of Fluorescent Acenequinones as Dyes for Guest-Host Liquid Crystal Displays. *Org. Lett.* **2007**, *9*, 997-1000.

24. Pellatt, M. G.; Roe, I. H. C.; Constant, J., Photostable Anthraquinone Pleochroic Dyes. *Mol. Cryst. Liq. Cryst.* **1980**, *59*, 299-316.

25. Saunders, F. C.; Harrison, K. J.; Raynes, E. P.; Thompson, D. J., New Photostable Anthraquinone Dyes with High Order Parameters. *IEEE Trans. Electron Devices* **1983**, *30*, 499-503.

26. Iwanaga, H.; Naito, K.; Nakai, Y., The Molecular Structures and Properties of Anthraquinone-Type Dichroic Dyes. *Mol. Cryst. Liq. Cryst.* **2001**, *364*, 211-218.

27. Bahadur, B., In *Handbook of Liquid Crystals*, Demus, D.; Goodby, J. W.; Gray, G. W.; Spiess, H. W.; Vill, V., Eds. Wiley-VCH: Weinheim, 1998; Vol. 2 A, pp 257-302.

28. Matsui, M.; Tanaka, N.; Andoh, N.; Funabiki, K.; Shibata, K.; Muramatsu, H.; Abe, Y.; Kaneko, M., Synthesis and Properties of Novel Dichroic Disazo Dyes Containing the Tetrafluoro-P-Phenylene Moiety for Guest−Host Liquid Crystal Displays. *Chem. Mater.* **1998**, *10*, 1921-1930.

29. Bahadur, B., In *Liquid Crystals: Applications and Uses*, Bahadur, B., Ed. World Scientific Publishing Co. Pte. Ltd.: Singapore, 1992; Vol. 3, pp 65-208.

30. Diaz, A. N., Absorption and Emission-Spectroscopy and Photochemistry of 1,10-Anthraquinone Derivatives - a Review. *J. Photochem. Photobiol. A* **1990**, *53*, 141-167.

31. Iwanaga, H., Development of Highly Soluble Anthraquinone Dichroic Dyes and Their Application to Three-Layer Guest-Host Liquid Crystal Displays. *Materials* **2009**, *2*, 1636-1661.

32. Iwanaga, H.; Naito, K.; Aiga, F., Properties of Novel Yellow Anthraquinone Dichroic Dyes with Naphthylthio Groups for Guest-Host Liquid Crystal Displays. *J. Mol. Struct.* **2010**, *975*, 110-114.

33. Cowling, S. J.; Ellis, C.; Goodby, J. W., Anthraquinone Liquid Crystal Dichroic Dyes – a New Form of Chromonic Dye? *Liq. Cryst.* **2011**, *38*, 1683-1698.

34. Sims, M. T.; Abbott, L. C.; Cowling, S. J.; Goodby, J. W.; Moore, J. N., Dyes in Liquid Crystals: Experimental and Computational Studies of a Guest–Host System Based on a Combined DFT and MD Approach. *Chem. - Eur. J.* **2015**, *21*, 10123-10130.

35. Harrison, K. J.; Raynes, E. P.; Saunders, F. C.; Thompson, D. J. Liquid Crystal Materials Containing Pleochroic Anthraquinone Dyes. US 4391489, 1983.

36. Harrison, K. J.; Raynes, E. P.; Saunders, F. C.; Thompson, D. J. Liquid Crystal Materials Comprising Pleochroic Dyes. EP 0059095 B1, 1987.

37. Constant, J.; Pellatt, M. G.; Roe, I. H. C. Pleochroic Dyes Suitable for Use in Solution with Liquid Crystal Materials for Electro-Optic Device Applications. EP 0002104 B1, 1982.

38. Thompson, D. J. Pleochroic Anthraquinone Dyes. US 4446047, 1984.

39. Gritzner, G.; Kůta, J., Recommendations on Reporting Electrode Potentials in Nonaqueous Solvents. *Electrochim. Acta* **1984**, *29*, 869-873.

40. R Core Team (2014). R: A language and environment for statistical computing. R Foundation for Statistical Computing, Vienna, Austria. URL http://www.R-project.org/.

41. Frisch, M. J., et al., Gaussian 09, Revision B.01. In *Gaussian 09, Revision B.01*, Gaussian Inc., Wallingford CT2009.

42. Becke, A. D., Density-Functional Thermochemistry .3. The Role of Exact Exchange. *J. Chem. Phys.* **1993**, *98*, 5648-5652.

43. Lee, C. T.; Yang, W. T.; Parr, R. G., Development of the Colle-Salvetti Correlation-Energy Formula into a Functional of the Electron-Density. *Phys. Rev. B* **1988**, *37*, 785-789.

44. Marenich, A. V.; Cramer, C. J.; Truhlar, D. G., Universal Solvation Model Based on Solute Electron Density and on a Continuum Model of the Solvent Defined by the Bulk Dielectric Constant and Atomic Surface Tensions. *J. Phys. Chem. B* **2009**, *113*, 6378-6396.

45. Bernath, P. F., *Spectra of Atoms and Molecules*; Oxford University Press, 2005.

46. Hansch, C.; Leo, A.; Taft, R. W., A Survey of Hammett Substituent Constants and Resonance and Field Parameters. *Chem. Rev.* **1991**, *91*, 165-195.

47. Zollinger, H., *Color Chemistry*, 3rd ed.; WILEY-VCH, 2003.

48. Braslavsky, S. E., Glossary of Terms Used in Photochemistry, 3rd Edition (Iupac Recommendations 2006). *Pure Appl. Chem.* **2007**, *79*, 293-465.

49. Bailey, M.; Brown, C. J., The Crystal Structure of N,N'-Diphenyl-1,5-Diaminoanthraquinone. *Acta Crystallogr.* **1966**, *22*, 488-492.

50. He, L.; Freeman, H. S.; Lu, L. H.; Zhang, S. F., Spectroscopic Study of Anthraquinone Dye/Amphiphile Systems in Binary Aqueous/Organic Solvent Mixtures. *Dyes Pigm.* **2011**, *91*, 389-395.

51. Gautrot, J. E.; Hodge, P.; Cupertino, D.; Helliwell, M., 2,6-Diaryl-9,10-Anthraquinones as Models for Electron-Accepting Polymers. *New J. Chem.* **2007**, *31*, 1585-1593.

52. Pelaez, J.; Wilson, M., Molecular Orientational and Dipolar Correlation in the Liquid Crystal Mixture E7: A Molecular Dynamics Simulation Study at a Fully Atomistic Level. *Phys. Chem. Chem. Phys.* **2007**, *9*, 2968-2975.

53. Capar, M. I.; Cebe, E., Molecular Dynamic Study of the Odd-Even Effect in Some 4-N-Alkyl-4'-Cyanobiphenyls. *Phys. Rev. E* **2006**, *73*, 061711.

54. Stroobants, A.; Lekkerkerker, H. N. W.; Frenkel, D., Evidence for One-Dimensional, Two-Dimensional, and 3-Dimensional Order in a System of Hard Parallel Spherocylinders. *Phys. Rev. A* **1987**, *36*, 2929-2945.

55. Veerman, J. A. C.; Frenkel, D., Relative Stability of Columnar and Crystalline Phases in a System of Parallel Hard Spherocylinders. *Phys. Rev. A* **1991**, *43*, 4334-4343.

56. Poniewierski, A., Nematic to Smectic-a Transition in the Asymptotic Limit of Very Long Hard Spherocylinders. *Phys. Rev. A* **1992**, *45*, 5605-5613.

57. Villanueva-Garcia, M.; Martinez-Richa, A.; Robles, J., Derivation by Electronic Structure Calculations of the Aspect Ratios (Length/Diameter) for Homologous Series of Calamitic Liquid Crystals. *Mol. Cryst. Liq. Cryst.* **2006**, *446*, 245-254.

58. Brown, J. T.; Allen, M. P.; Martín del Río, E.; Miguel, E. d., Effects of Elongation on the Phase Behavior of the Gay-Berne Fluid. *Phys. Rev. E* **1998**, *57*, 6685-6699.

59. Shamsipur, M.; Hemmateenejad, B.; Babaei, A.; Faraj-Sharabiani, L., Use of Multivariate Curve Resolution Analysis in the Spectroelectrochemistry of 9,10-Anthraquinone Reduction in Dimethylformamide Solution. *J. Electroanal. Chem.* **2004**, *570*, 227-234.

60. DeAngelis, T. P.; Heineman, W. R., An Electrochemical Experiment Using an Optically Transparent Thin Layer Electrode. *J. Chem. Educ.* **1976**, *53*, 594-597.

61. Shamsipur, M.; Siroueinejad, A.; Hemmateenejad, B.; Abbaspour, A.; Sharghi, H.; Alizadeh, K.; Arshadi, S., Cyclic Voltammetric, Computational, and Quantitative Structure-Electrochemistry Relationship Studies of the Reduction of Several 9,10-Anthraquinone Derivatives. *J. Electroanal. Chem.* **2007**, *600*, 345-358.

62. Shamsipur, M.; Alizadeh, K.; Arshadi, S., Computational Electrochemistry of Aqueous Two-Electron Reduction Potentials of Some Amino-9,10-Anthraquinone Derivatives. *J. Mol. Struct.: Theochem* **2006**, *758*, 71-74.

63. Alizadeh, K.; Shamsipur, M., Calculation of the Two-Step Reduction Potentials of Some Quinones in Acetonitrile. *J. Mol. Struct.: Theochem.* **2008**, *862*, 39-43.

64. Davis, A. P.; Fry, A. J., Experimental and Computed Absolute Redox Potentials of Polycyclic Aromatic Hydrocarbons Are Highly Linearly Correlated over a Wide Range of Structures and Potentials. *J. Phys. Chem. A* **2010**, *114*, 12299-12304.

65. Konezny, S. J.; Doherty, M. D.; Luca, O. R.; Crabtree, R. H.; Soloveichik, G. L.; Batista, V. S., Reduction of Systematic Uncertainty in DFT Redox Potentials of Transition-Metal Complexes. *J. Phys. Chem. C* **2012**, *116*, 6349-6356.

66. Lehmann, M. W.; Evans, D. H., Anomalous Behavior in the Two-Step Reduction of Quinones in Acetonitrile. *J. Electroanal. Chem.* **2001**, *500*, 12-20.

67. Eberson, L.; Hartshorn, M. P., On the Existence of Quinone Radical Cations. A Study in 1,1,1,3,3,3-Hexafluoropropan-2-Ol. *J. Chem. Soc., Perkin Trans. 2* **1996**, 151-154.

68. Pommerehne, J.; Vestweber, H.; Guss, W.; Mahrt, R. F.; Bässler, H.; Porsch, M.; Daub, J., Efficient Two Layer Leds on a Polymer Blend Basis. *Adv. Mater.* **1995**, *7*, 551-554.

69. Thelakkat, M.; Schmidt, H.-W., Synthesis and Properties of Novel Derivatives of 1,3,5-Tris(Diarylamino)Benzenes for Electroluminescent Devices. *Adv. Mater.* **1998**, *10*, 219-223.

70. Brownell, L. V.; Robins, K. A.; Jeong, Y.; Lee, Y.; Lee, D. C., Highly Systematic and Efficient Homo-Lumo Energy Gap Control of Thiophene-Pyrazine-Acenes. *J. Phys. Chem. C.* **2013**, *117*, 25236-25247.

71. Homnick, P. J.; Tinkham, J. S.; Devaughn, R.; Lahti, P. M., Engineering Frontier Energy Levels in Donor–Acceptor Fluoren-9-Ylidene Malononitriles Versus Fluorenones. *J. Phys. Chem. A* **2013**, *118*, 475-486.

72. Görner, H., Photoreduction of 9,10-Anthraquinone Derivatives: Transient Spectroscopy and Effects of Alcohols and Amines on Reactivity in Solution. *Photochem. Photobiol.* **2003**, *77*, 171-179.

Table of Contents Image